Cell, Vol. 115, 863–877, December 26, 2003, Copyright ©2003 by Cell Press

A Key Role for TRPM7 Channels in Anoxic Neuronal Death

Michelle Aarts,[1,4] Koji Iihara,[1,4] Wen-Li Wei,[2,4] Zhi-Gang Xiong,[2] Mark Arundine,[1] Waldy Cerwinski,[2] John F. MacDonald,[2] and Michael Tymianski[1,2,3,*]

[1]Toronto Western Hospital Research Institute
11-416 MC-PAV
399 Bathurst Street
Toronto, Ontario
M5T-2S8
Canada

[2]Department of Physiology

[3]Department of Surgery
University of Toronto
Toronto, Ontario
M5S-1A8
Canada

Summary

Excitotoxicity in brain ischemia triggers neuronal death and neurological disability, and yet these are not prevented by antiexcitotoxic therapy (AET) in humans. Here, we show that in neurons subjected to prolonged oxygen glucose deprivation (OGD), AET unmasks a dominant death mechanism perpetuated by a Ca^{2+}-permeable nonselective cation conductance (I_{OGD}). I_{OGD} was activated by reactive oxygen/nitrogen species (ROS), and permitted neuronal Ca^{2+} overload and further ROS production despite AET. I_{OGD} currents corresponded to those evoked in HEK-293 cells expressing the nonselective cation conductance TRPM7. In cortical neurons, blocking I_{OGD} or suppressing TRPM7 expression blocked TRPM7 currents, anoxic $^{45}Ca^{2+}$ uptake, ROS production, and anoxic death. TRPM7 suppression eliminated the need for AET to rescue anoxic neurons and permitted the survival of neurons previously destined to die from prolonged anoxia. Thus, excitotoxicity is a subset of a greater overall anoxic cell death mechanism, in which TRPM7 channels play a key role.

Introduction

Excitotoxicity is the process by which L-glutamate, the major excitatory neurotransmitter in the mammalian CNS, damages neurons (Olney, 1969). It is established as a predominant neurotoxic mechanism in acute neurological disorders such as stroke, epilepsy, and traumatic nervous system injuries (Lipton and Rosenberg, 1994). In brain ischemia, excitotoxic glutamate receptor activity triggers several damaging processes, of which Ca^{2+} influx through *N*-methyl-*D*-aspartate glutamate receptors (NMDARs) is key (reviewed in Lipton, 1999). Blocking NMDARs permitted neurons destined to die from anoxia to survive (Goldberg et al., 1987), and animal research suggested that this approach could be used to treat ischemic brain damage (Simon et al., 1984). However, clinical trials of antiexcitotoxic therapy (AET) have generally failed to benefit patients (Davis et al., 1997; Morris et al., 1999; Lees et al., 2000). The paradoxical failure of AET in the face of a clear role for excitotoxicity in acute neurological disorders is unexplained (Birmingham, 2002; Ikonomidou and Turski, 2002).

To probe this problem, we examined whether a neurotoxic process other than excitotoxicity might have been overlooked. We returned to experiments in cultured murine cortical neurons, an established system used to derive fundamental principles of excitotoxicity (Goldberg et al., 1987; Choi et al., 1987; Sattler et al., 1998, 1999; Aarts et al., 2002). The cultures were exposed to oxygen-glucose deprivation (OGD), reported to mediate neuronal death through NMDAR activation (Goldberg et al., 1987; Goldberg and Choi, 1993). Here, we show that AET in anoxic neurons unmasks a lethal cation current I_{OGD} mediated by TRPM7, a member of the transient receptor potential cation channel superfamily (Nadler et al., 2001; reviewed in Montell et al., 2002). In OGD, I_{OGD} is activated by reactive oxygen/nitrogen species (ROS), permitting Ca^{2+} uptake that further stimulates ROS and I_{OGD} activation. Blocking I_{OGD} or suppressing TRPM7 expression prevents anoxic neuronal death even in the absence of AET, indicating that TRPM7 is an essential mediator of anoxic death. This work defines a paradigm for understanding anoxic neuronal damage in which excitotoxicity is a subset of a larger framework.

Results

Prolonged OGD Causes Ca^{2+}-Dependent Neurotoxicity Despite AET

We first reproduced the studies that implicated excitotoxicity in anoxic neuronal death. Cultured cortical neurons were exposed to OGD and treated with glutamate antagonists. Excitotoxic neuronal death and $^{45}Ca^{2+}$ uptake can be eliminated by treating these cells with MK-801 (10 μM), CNQX (10 μM), and nimodipine (2 μM), antagonists of NMDA and AMPA/kainate glutamate receptors and L-type Ca^{2+} channels, respectively (Sattler et al., 1998, 1999; Aarts et al., 2002). Accordingly, we reasoned that this combination (hereafter abbreviated as MCN) would be similarly effective in OGD (hereafter denoted as OGD_{MCN}). Consistent with previous studies, all untreated neurons succumbed to a 1 hr OGD insult by 24 hr, but could be rescued if treatment was undertaken using any antagonist combination that included MK-801 (10 μM; Figures 1A and 1E$_1$; Goldberg and Choi, 1993). However, AET failed to prevent neuronal death if OGD was extended to 1.5 hr or more, even with all three antagonists present (Figures 1A and 1E$_2$). Separate experiments suggested that this death is necrotic, without evidence of apoptosis (see Supplemental Data available at http://www.cell.com/cgi/content/full/115/7/863/DC1). MCN is thus insufficient to rescue neurons from prolonged OGD.

*Correspondence: mike_t@uhnres.utoronto.ca
[4]These authors contributed equally to this work.

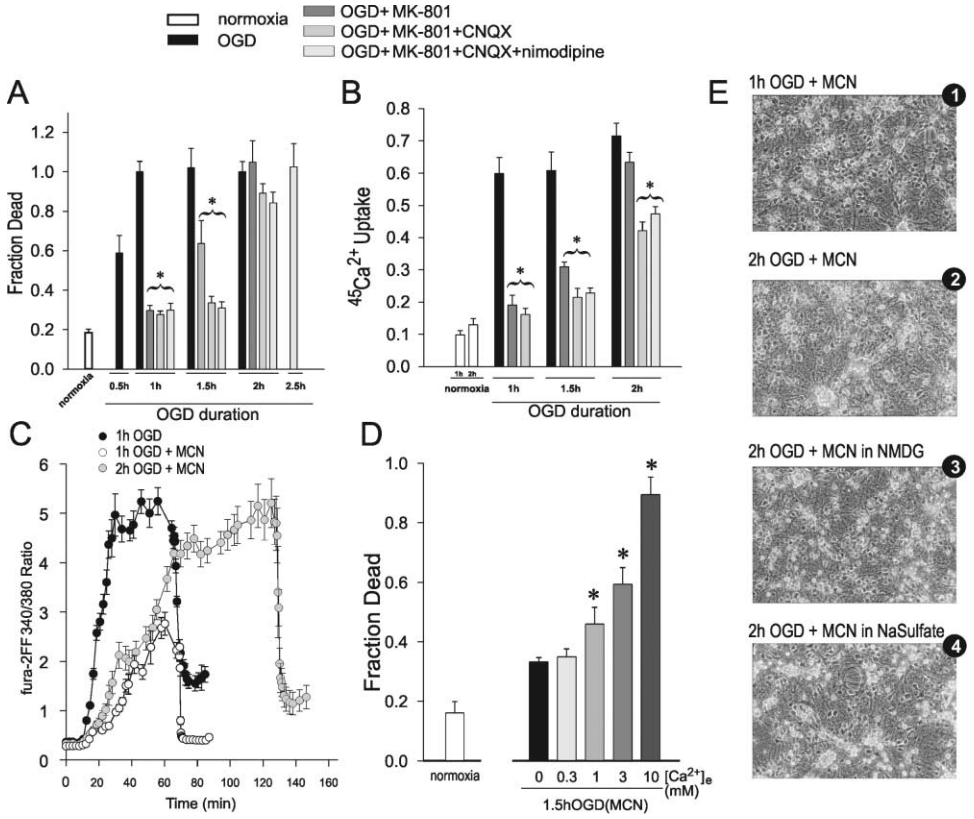

Figure 1. Treating Excitotoxicity and Blocking Ca^{2+} Channels Is Insufficient to Prevent Ca^{2+}-Influx-Dependent Neuronal Death in Prolonged OGD

(A and B) Effect of OGD duration and the indicated antagonists on neuroprotection (A) and $^{45}Ca^{2+}$ accumulation.

(B) Asterisk (*): different from OGD without antagonists in same group (ANOVA, $p < 0.01$). Scale bars are equal to mean + SEM of 18–28 cultures from four experiments.

(C) Effect of MCN on the OGD-evoked rise in $[Ca^{2+}]_i$ measured with fura 2-FF. Symbols are equal to mean ± SEM from five experiments.

(D) Neuronal death 22.5 hr after a 1.5 hr OGD in MCN and the indicated $[Ca^{2+}]_e$. Scale bars are equal to mean + SEM of 12 cultures from two experiments. Asterisk: difference from zero $[Ca^{2+}]_e$ (Bonferroni t test, $p < 0.0015$).

(E) Representative phase images of cultures 24 hr post OGD with MCN. Images: (1) 1 hr OGD; (2) 2 hr OGD; (3) 2 hr OGD, NaCl substituted with NMDG; and (4) 2 hr OGD, NaCl substituted with Na Sulfate.

As the MCN combination blocks all Ca^{2+} influx elicited by excitotoxins (Sattler et al., 1998), we reasoned that cell death in prolonged OGD_{MCN} might involve Ca^{2+}-independent mechanisms. To test this we measured neuronal $^{45}Ca^{2+}$ uptake and free intracellular Ca^{2+} concentration ($[Ca^{2+}]_i$) during OGD. In the absence of MCN, OGD for 1 hr evoked the anticipated, significant, neuronal $^{45}Ca^{2+}$ uptake (Goldberg and Choi, 1993), and this was blocked by any antagonist combination containing MK-801 (Figure 1B). Surprisingly however, blocking glutamate receptors and Ca^{2+} channels did not prevent $^{45}Ca^{2+}$ uptake in the second hour of OGD. After 2 hr, $^{45}Ca^{2+}$ uptake in neurons treated with MCN almost matched that of untreated cells. Next, $[Ca^{2+}]_i$ measurements were made with the low Ca^{2+}-affinity indicator Fura-2/FF (Experimental Procedures). OGD in the absence of MCN elicited a rapid rise in $[Ca^{2+}]_i$ that recovered upon reoxygenation (Figure 1C). Treatment with MCN slowed this rise and, in neurons exposed to 1 hr OGD, allowed $[Ca^{2+}]_i$ to recover to baseline. However, increasing the OGD duration permitted a further $[Ca^{2+}]_i$ rise despite MCN treatment. By 2 hr, $[Ca^{2+}]_i$ in neurons subjected to OGD_{MCN} matched that of neurons subjected to 1 hr OGD without antagonists (Figure 1C) . Thus, MCN is insufficient to prevent a loss of neuronal Ca^{2+} homeostasis in prolonged OGD.

Next, we determined the ionic dependence of neuronal death in prolonged OGD_{MCN}. As death correlated with extracellular $^{45}Ca^{2+}$ uptake (Figures 1A and 1B), we first exposed the cultures to 1.5 hr OGD_{MCN} in a range of extracellular Ca^{2+} concentrations ($[Ca^{2+}]_e$; Figure 1D). This revealed a dependence of cell death on $[Ca^{2+}]_e$, implicating Ca^{2+} influx as a cause. To determine contributions from other ions, we studied neuronal damage and $^{45}Ca^{2+}$ accumulation in 2 hr OGD_{MCN} during extracellular Na^+ or Cl^- removal or extracellular K^+ supplementation. Neither neuronal death 24 hr after 2 hr OGD_{MCN} nor $^{45}Ca^{2+}$ uptake at 2 hr was reduced by these procedures (Supplemental Table S1 available on *Cell* website; Figure 1E). Thus, disturbances involving Na^+, Cl^-, or K^+ are unlikely to contribute to the toxicity unmasked by prolonging OGD in the face of AET, whereas Ca^{2+} influx is key.

Excitotoxicity May Be Self-Limiting

As AET became increasingly ineffective after 1 hr OGD_{MCN}, we used whole-cell recordings to probe the time course of glutamate release and NMDAR activation.

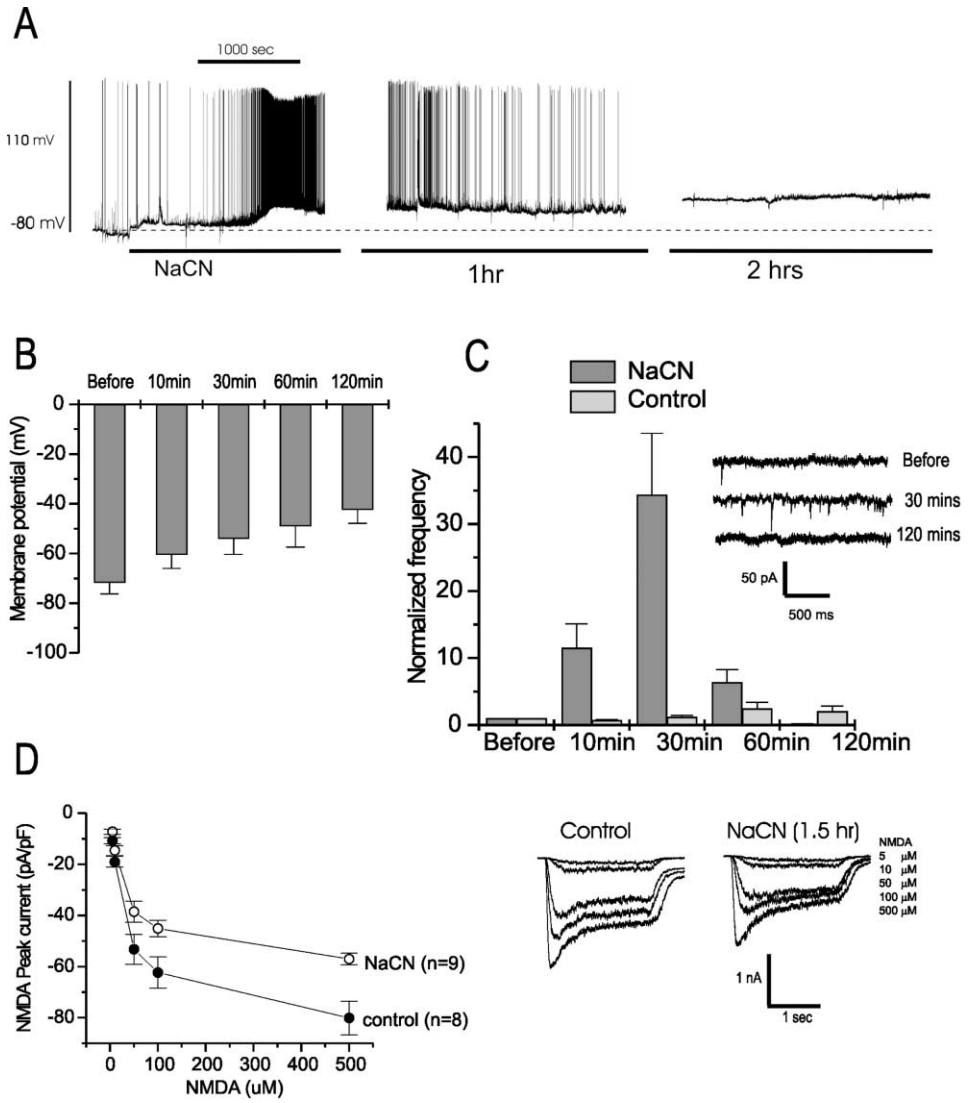

Figure 2. Prolonged Anoxia Inhibits Synaptic Glutamate Release and NMDAR Activity

(A and B) Current clamp recordings (A) and membrane potential (B) of cultured neurons during NaCN treatment (3 mM, in glucose-free ECF, 10 μM bicuculline, no TTX). Neurons remain depolarized but all spontaneous activity is lost by 2 hr. (mean ± SE, n = 4).

(C) Frequency of miniature excitatory synaptic currents (epscs, mean ±, SE n = 5) under voltage clamp (holding −60 mV). Action potentials were blocked with TTX (300 nM) and inhibitory GABA currents with bicuculline (10 μM). Threshold detection of miniatures was done manually and was at least twice the baseline noise. Inset: sample recordings.

(D) Concentration-dependent NMDA currents in control and NaCN (3 mM, in glucose free ECF, incubated for 1.5 hr) treated neurons. Holding potential was −60 mV. Glycine = 0.5 μM. Symbols are equal to mean ± SE. Insets: sample currents at the indicated NMDA concentrations. Recording solutions in (A–D) in mM: current clamp ICF, KCl 140, $MgCl_2$ 2, $CaCl_2$ 1, EGTA 11, HEPES 10, and K_2ATP 2; voltage clamp ICF, CsCl 140, MgCl2 2, CaCl2 1, TEA-Cl 2, EGTA 11, HEPES 10, K2ATP 2, and [pH 7.3]; ECF, NaCl 140, KCl 5.4, $CaCl_2$ 1.3, HEPES 25, glucose 33, and [pH 7.4]. Glucose-free ECF made by substituting glucose with NMDG. EGTA and $CaCl_2$ were omitted from the patch pipette in (D).

The cultures were treated with NaCN (3 mM) in glucose-free ECF to simulate anoxia/aglycemia. This initially evoked a depolarization and increased synaptic glutamate release (Figure 2A), also evidenced as an increase in the frequency of miniature excitatory synaptic currents (mEPSC; Figure 2C). However, by 2 hr the excitation and glutamate release ceased as the neurons remained depolarized (Figures 2A and 2B), and the mEPSC frequency fell to zero (Figure 2C). Adding APV (50 μM) and CNQX (10 μM) at 1.5 hr had no effect on the membrane potential (data not shown), suggesting against ongoing nonsynaptic glutamate release (Rossi et al., 2000). Also, treatment with NaCN (3 mM for 1.5 hr) depressed currents evoked by NMDA (0–500 μM) following washout of NaCN, suggesting NMDAR inactivation (Figure 2D). These data imply that excitotoxicity becomes less pronounced when anoxia is prolonged, consistent with the reduced neuroprotection by MCN in this time frame.

Prolonged Anoxia/Aglycemia Activates a Distinct Cation Conductance

To determine the route of lethal Ca^{2+} influx in 2 hr OGD_{MCN}, we next probed conventional pathways reported to participate in OGD-induced neuronal Ca^{2+} uptake. However, agonists or antagonists of glutamate

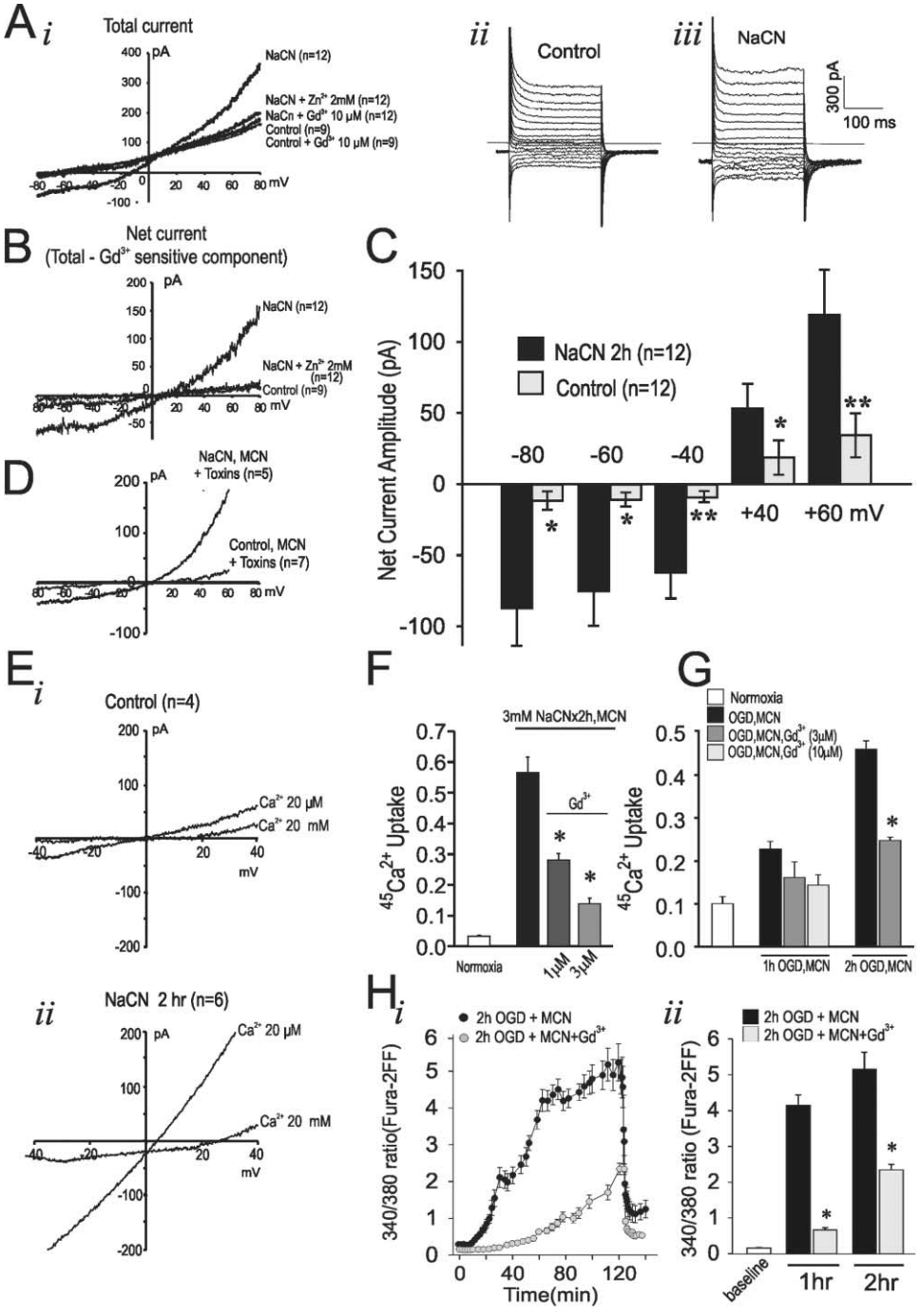

Figure 3. Exposure of Neurons to OGD or Chemical Anoxia (NaCN) in MCN Induces a Distinct Cation Current

I-V curve measurements in (A–E) were obtained after a 2 hr NaCN exposure, and averaged from the indicated (n) number of neurons.

(A) I-V curves (*i*) and sample traces (*ii, iii*) of the enhancement in total inward and outward currents by NaCN. The portion enhanced by NaCN is sensitive to block by Gd^{3+} and Zn^{2+}.

(B) I-V curve of the net current induced by NaCN exposure (Gd^{3+} sensitive component only).

(C) Summary of the effect of NaCN at different membrane potentials. Net current was obtained by subtracting the total current in the presence of 10 μM Gd^{3+} from that without Gd^{3+}. Asterisks: differences from NaCN exposed neurons in the same voltage group (Bonferroni t test, *$p < 0.01$).

(D) Lack of effect of the Ca^{2+} channel toxins ω-Conotoxin GVIA (500 nM) and ω-Agatoxin-TK (200 nM) to MCN on the NaCN-induced current.

(E) I-V curves of net Gd^{3+}-sensitive current in controls (*i*) and NaCN-treated (*ii*) neurons in the presence of low (20 μM) and high (20 mM) $[Ca^{2+}]_e$. Changing $[Ca^{2+}]_e$ from low to high shifted the reversal potential from 3.2 ± 2.5 mV to 19.2 ± 5.8 mV ($n = 6$, $p < 0.05$).

(F) Effect of Gd^{3+} on $^{45}Ca^{2+}$ uptake during a 2 hr exposure to NaCN in MCN.

(G) Effect of Gd^{3+} on $^{45}Ca^{2+}$ uptake during OGD.

(H) Blocking effect of Gd^{3+} on the rise in $[Ca^{2+}]_i$ during OGD. (*i*) Averaged traces derived from 5 experiments (Symbols: mean ± SEM). (*ii*) Effect of Gd^{3+} on peak $[Ca^{2+}]_i$ at the indicated times (five experiments per scale bar, mean + SEM). Asterisk: different from OGD without Gd^{3+} in the same group (Student's t test, $p < 0.001$).

receptors, voltage-sensitive Ca^{2+} or Na^{+} channels, ion exchangers, and others had no effect on $^{45}Ca^{2+}$ uptake or cell death (see Supplemental Data available on *Cell* website). Thus, we hypothesized that a previously overlooked conductance was involved. To facilitate its identification, we performed further patch-clamp recordings in neurons subjected for 2 hr to chemical anoxia/aglycemia in 3 mM NaCN and MCN (hereafter denoted as $NaCN_{MCN}$). This evoked a cation current that exceeded the baseline leak current in all neurons (Figure 3A*$_{i–iii}$*). The evoked current could be blocked by Gd^{3+} (10 μM) or Zn^{2+} (2 mM), polyvalent cations that inhibit a range of nonselective cation conductances (Figure 3A). The net I-V relationship (total minus Gd^{3+}-sensitive component; Figures 3B and 3C) was studied in the remaining experiments. Its outward rectification at positive potentials and reversal potential near 0 mV suggested a nonselective cation channel. It was not carried by voltage dependent Ca^{2+} channels as it was unaffected by membrane voltage (Figures 3A and 3B) nor by nimodipine (present in MCN) with ω-conotoxin G*VI*A (500 nM) and ω-agatoxin *IV*A (200 nM), blockers of L, N, and P/Q type Ca^{2+}-channels, respectively (Figure 3D). Changing $[Ca^{2+}]_e$ from low (20 μM) to high (20 mM) shifted its reversal potential from 3.2 ± 2.5 mV to 19.2 ± 5.8 mV ($n = 6$, $p < 0.05$), suggesting that the current is carried in part by Ca^{2+} (Figure 3E*$_{i,ii}$*). Also, lowering $[Ca^{2+}]_e$ dramatically increased the magnitude of both inward and outward currents, and produced a more linear I-V curve, suggesting a sensitivity to low $[Ca^{2+}]_e$ and conductance to monovalent cations (Figure 3E*$_{ii}$*).

To determine whether the cation current elicited by $NaCN_{MCN}$ and the $^{45}Ca^{2+}$ uptake elicited by OGD_{MCN} were related, we examined whether Gd^{3+}, which blocked the current (Figure 3A), also affected Ca^{2+} uptake. Gd^{3+} (1–3 μM) blocked both $^{45}Ca^{2+}$ uptake (Figure 3F) and $[Ca^{2+}]_i$ elevations (data not shown) evoked by 2 hr $NaCN_{MCN}$. Gd^{3+} also attenuated $^{45}Ca^{2+}$ uptake and $[Ca^{2+}]_i$ elevations evoked by 2 hr OGD_{MCN} (Figures 3G and 3H*$_{i,ii}$*), suggesting that the $NaCN_{MCN}$-evoked current and the OGD_{MCN}-evoked Ca^{2+} uptake may occur by similar mechanisms. Therefore, the conductance responsible for both is hereafter termed I_{OGD}.

The I_{OGD} current could be recorded after 2 hr $NaCN_{MCN}$ prior to any morphological alterations in the neurons (data not shown) and without detectable changes in membrane surface area as calculated from capacitive transients in all recordings (data not shown). This and the block of I_{OGD} by Gd^{3+} (Figures 3A, 3F, 3G, and 3H) argue against I_{OGD} being due to nonspecific membrane breakdown that raises a neuron's permeability to cations.

Reactive Oxygen Species Trigger I_{OGD} Currents and Ca^{2+} Uptake in Prolonged OGD

Excitotoxicity and anoxia each elicit neurotoxic reactive oxygen species (ROS) production (Lipton, 1999). As prolonged OGD_{MCN} is toxic despite AET (Figure 1), we examined whether ROS were involved. Neuronal ROS are produced by three principal pathways. In the first, ferrous iron catalyses the decomposition of peroxides, yielding OH· from H_2O_2 (hereafter termed the "iron" pathway). In the second, oxidative metabolism of phospholipid-derived arachidonic acid occurs via the cyclooxygenase or lipoxygenase pathways and leads to O_2^- or OH· production (hereafter termed the "arachidonic acid" pathway). In the third, neuronal nitric oxide synthase (nNOS) produces nitric oxide (NO), which combines with mitochondrially, derived O_2^- anion to form peroxynitrite radicals (hereafter termed the "NO" pathway). We examined the role of each in triggering I_{OGD} currents and $^{45}Ca^{2+}$ uptake in anoxia.

First we evaluated the effects of antioxidants on I_{OGD} currents. Neurons were treated with 6-hydroxy-2,5,7,8-tetramethylchroman-2-carboxylate (trolox; 1 mM), a water-soluble form of α-tocopherol (vitamin E), or with manganese (III) tetrakis (4-benzoic acid) porphyrin (MnTBAP; 200 μM), an O_2^- scavenger (Patel et al., 1996). Each attenuated both I_{OGD} currents in 2 hr $NaCN_{MCN}$ (Figure 4A) and $^{45}Ca^{2+}$ uptake during 2 hr OGD_{MCN} (Figure 4C). This suggests I_{OGD} activation by ROS, and that O_2^- is involved.

Next, we examined the impact of "iron" pathway modulators. I_{OGD} in 2 hr $NaCN_{MCN}$ and $^{45}Ca^{2+}$ uptake in 2 hr OGD_{MCN} were unaffected by treatment with desferoxamine, an iron chelator which should reduce the catalysis of H_2O_2 to OH· by Fe^{2+} (Figures 4B and 4D). $^{45}Ca^{2+}$ uptake was also unaffected by adding Fe^{2+} to enhance OH· production (Figure 4D). Also, adding catalase (30–300 U/ml) to decompose peroxides to H_2O had no effect (data not shown). Thus, ROS that activate I_{OGD} are not likely generated by the iron pathway.

We next tested inhibitors of the various components of the arachidonic acid pathway. U73122 (a phospholipase-C inhibitor) and $AACOCF_3$ (a phospholipase A2 inhibitor), inhibit arachidonate production from phospholipid breakdown. Indomethacin (Indocid) is a cyclooxygenase inhibitor at 10 μM and PLA_2 inhibitor at 300 μM). Baicalain (5 μM) and norhydroguaiaretic acid (NDGA; 10μM) each inhibit lipoxygenase. These should reduce O_2^- and OH· formation from arachidonate metabolism. However, none affected $^{45}Ca^{2+}$ uptake after 2 hr OGD_{MCN} (Figure 4C), suggesting that the arachidonate pathway is also unlikely to generate the ROS that activate I_{OGD}.

To examine the involvement of endogenous ROS in activating I_{OGD} directly, the cultures were challenged with menadione (150 μM), a mitochondrial O_2^- generator (Ying et al., 2000). This was compared to adding H_2O_2, or the combination of oligomycin (10 μM; ATP synthase inhibitor) and rotenone (5 μM; the mitochondrial complex I inhibitor) to collapse the mitochondrial membrane potential without affecting ATP/ADP ratios (Budd and Nicholls, 1996). All treatments evoked neuronal $^{45}Ca^{2+}$ uptake, which could be inhibited by Gd^{3+} (1–3 μM; Figure 4E). Similar results were obtained with oligomycin without rotenone (data not shown). Also, H_2O_2 activated a cation current with I-V characteristics matching I_{OGD} (Figure 4E, inset).

Although both the iron and the arachidonic acid pathways can produce H_2O_2 and other ROS, modulators of neither had effects on I_{OGD} currents or $^{45}Ca^{2+}$ uptake during 2 hr $NaCN_{MCN}$ or 2 hr OGD_{MCN} (Figures 4B, 4C, and 4D). We reason that in anoxia, these pathways may not induce sufficient ROS to activate I_{OGD}.

Next, we studied the involvement of NO signaling using whole-cell patch and $^{45}Ca^{2+}$ uptake measurements.

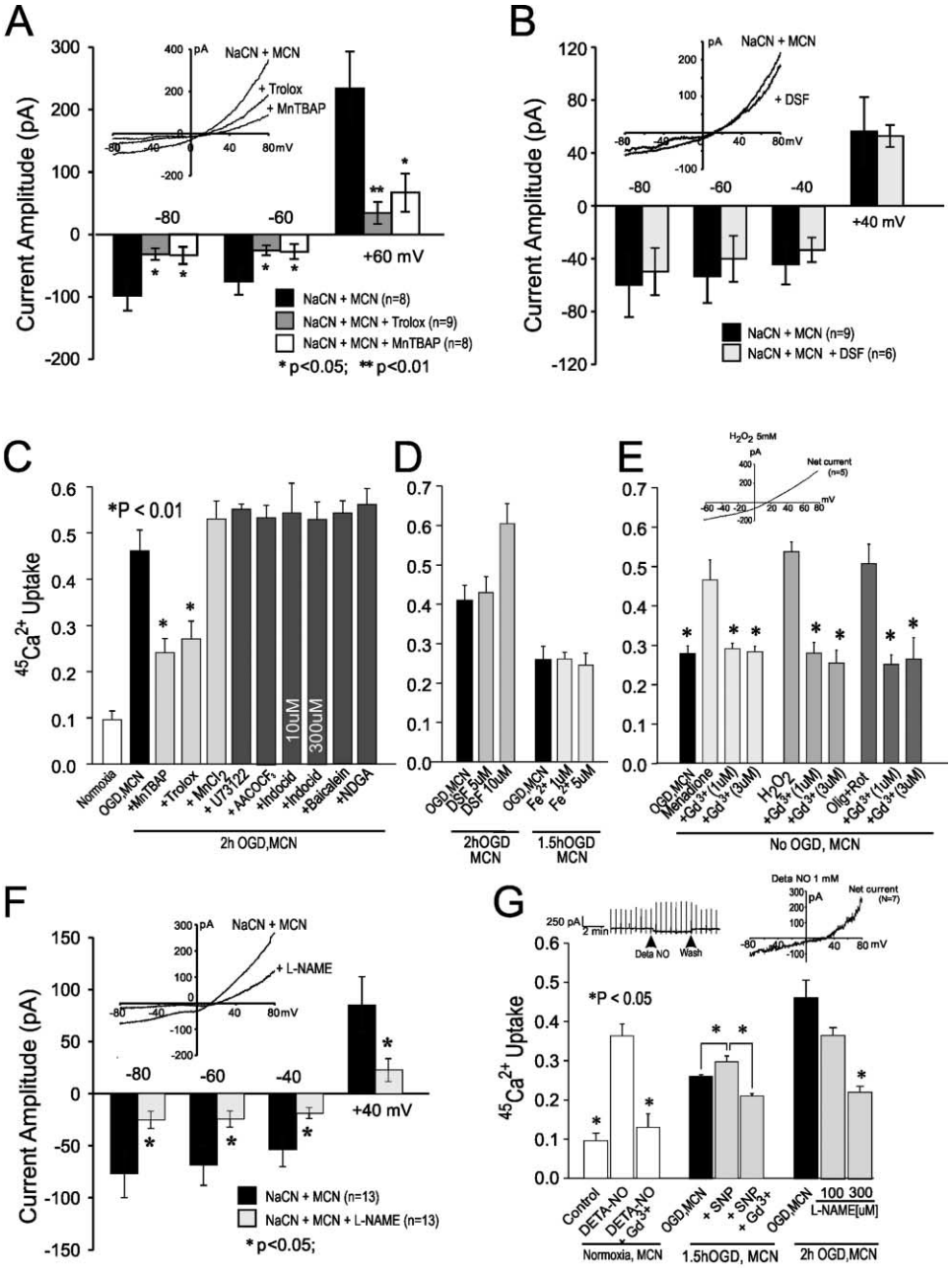

Figure 4. The Cation Current and $^{45}Ca^{2+}$ Uptake Evoked by OGD and NaCN Are Blocked by ROS Inhibitors Selective to the O_2^- and NO Pathways

All experiments were performed in MCN.

(A) Summary and averaged I-V curves (inset) of the effect of the ROS scavengers MnTBAP (0.2 mM) and trolox (1 mM) on the current evoked by NaCN.

(B) Lack of effect of desferoxamine (50 μM; DSF), an iron chelator, on the current evoked by NaCN.

(C) Inhibition by MnTBAP and trolox, but not by other antagonists of ROS pathways of $^{45}Ca^{2+}$ uptake evoked by OGD. Asterisk: different from OGD without antagonists, $p < 0.001$.

(D) Lack of effect of DSF in blocking, and of Fe^{2+} in enhancing, OGD-evoked $^{45}Ca^{2+}$ uptake.

(E) Effectiveness of Gd^{3+} in blocking menadione, oligomycin (Olig) + Rotenone (Rot)- and H_2O_2-evoked $^{45}Ca^{2+}$ uptake. Inset: net current evoked by H_2O_2. Asterisk: different from control in same group, (Bonferroni t test, $p < 0.001$).

(F) Summary and averaged I-V curves (inset) of the effect of the nNOS inhibitor L-NAME (300 μM) on the current evoked by NaCN.

(G) Effects of the NO donors DETA-NO (1 mM) and sodium nitroprusside (SNP; 1 mM), and of Gd^{3+} (3 μM) and L-NAME on $^{45}Ca^{2+}$ uptake under the indicated conditions. Asterisk: different from $^{45}Ca^{2+}$ uptake evoked alone. Inset: sample tracing and averaged I-V curve of net current evoked by DETA-NO. Scale bars in (C), (D), (E), and (G) are equal to mean + SEM of a minimum of three separate experiments.

The cultures were exposed to 2 hr $NaCN_{MCN}$ or 2 hr OGD_{MCN} in the presence of N^G-nitro-L-arginine methyl ester (L-NAME; 300 μM), a NOS inhibitor that protects these cells against excitotoxicity (Sattler et al., 1999). L-NAME inhibited both the cation current (Figure 4F) and $^{45}Ca^{2+}$ uptake (Figure 4G), implicating NO in I_{OGD}

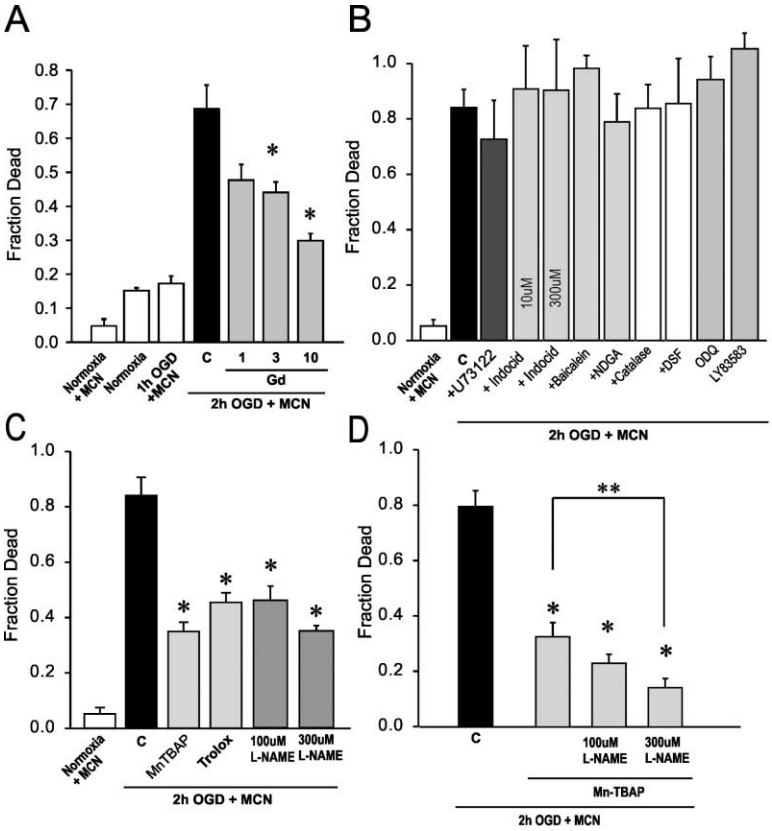

Figure 5. Inhibitors of I_{OGD} Permit the Survival of Neurons Otherwise Destined to Die from Prolonged OGD

Cultured neurons were exposed to 2 hr OGD in MCN. Cell death was gauged 22 hr thereafter.

(A) Neuroprotection by Gd^{3+}.

(B) No effect of inhibitors of ROS signaling not involving O_2^- and NO pathways.

(C) Neuroprotection by inhibitors of O_2^- and NO pathways.

(D) Synergistic protective effect of O_2^- and nNOS inhibition, ** $p < 0.05$, $n = 12$ experiments. Scale bars in (A–D) are equal to mean + SEM of ≥6 separate experiments. Asterisks: differences from control (c).

activation. Also, treating the cultures with the NO donors sodium nitroprusside (SNP; 500 μM) or (Z)-1-[2-(2-aminoethyl)-N-(2-ammonioethyl) amino]diazen-1-ium-1,2-diolate (DETA-NO; 500 μM) caused a $^{45}Ca^{2+}$ uptake, and this could be inhibited by Gd^{3+}. DETA-NO also activated a cation current with I-V characteristics matching I_{OGD} (Figure 4G, inset). Thus, of the three ROS pathways tested, the NO pathway activates I_{OGD} preferentially. This may be due to the reactive nitrogen species or to a larger overall quantity of ROS produced.

Blocking I_{OGD} Rescues Neurons

We next asked whether inhibiting I_{OGD} could rescue neurons exposed to prolonged OGD_{MCN} (Figure 1A). First we used Gd^{3+}, the direct blocker of I_{OGD} currents and $^{45}Ca^{2+}$ uptake (Figure 2). This reduced cell death caused by 2 hr OGD_{MCN} in a concentration-dependent manner (Figure 5A). As I_{OGD} currents and $^{45}Ca^{2+}$ uptake were best activated by ROS from the NO pathway, we examined whether the NO pathway, as compared with the others, also mediated the anoxic death. Inhibitors of the arachidonic acid and iron pathways were ineffective in attenuating cell death in OGD_{MCN} (Figure 5B). This was consistent with these compounds' inefficacy in inhibiting I_{OGD} currents or $^{45}Ca^{2+}$ uptake evoked by $NaCN_{MCN}$ and OGD_{MCN} (Figure 4). Thus, we focused on MnTBAP, trolox, and L-NAME either separately (Figure 5C) or in combination (Figure 5D). Each inhibited I_{OGD} and $^{45}Ca^{2+}$ uptake during $NaCN_{MCN}$ and OGD_{MCN} insults. Consistent with this, each protected neurons against anoxic death in OGD_{MCN} (Figures 5C and 5D). These results show that inhibiting I_{OGD}, either directly or indirectly, attenuates ROS production and Ca^{2+} influx and spares neurons that are otherwise destined to die from anoxia despite AET.

TRPM7 Is a Possible Primary Candidate for I_{OGD}

We next sought a possible candidate for I_{OGD}, a cation conductance that exhibits anoxia-induced currents with Ca^{2+} permeability, an outwardly rectifying I-V curve, enhancement by ROS and by low $[Ca^{2+}]_e$, and block by Gd^{3+}. We focused on transient receptor potential (TRP) cation channels, a family of about 20 mammalian proteins united by a common primary structure and permeability to monovalent cations and Ca^{2+}. A TRP channel family member, TRPM2, shows a linear I-V relationship and is regulated by ROS. In heterologous cells, TRPM2 expression enhances and TRPM2 suppression reduces, vulnerability to H_2O_2 toxicity (Hara et al., 2002). Also interesting is TRPM7, a cation channel containing a functional C-terminal kinase domain (Runnels et al., 2001; Nadler et al., 2001). TRPM7 currents in cell lines are activated at low MgATP levels (Nadler et al., 2001; Monteilh-Zoller et al., 2003), and are blocked by intracellular Mg^{2+} and Zn^{2+} (Kozak and Cahalan, 2003). These divalent cations both permeate TRPM7 channels and block the monovalent cation flow through them (Kerschbaum et al., 2003). Their regulation by redox modulators is not reported. However, heterologously overexpressed TRPM7 channels in HEK-293 cells exhibit currents with a high Ca^{2+} permeability, an outwardly rectifying I-V curve, enhancement by low $[Ca^{2+}]_e$, and block of monovalent currents by Gd^{3+}. Moreover, their overexpression

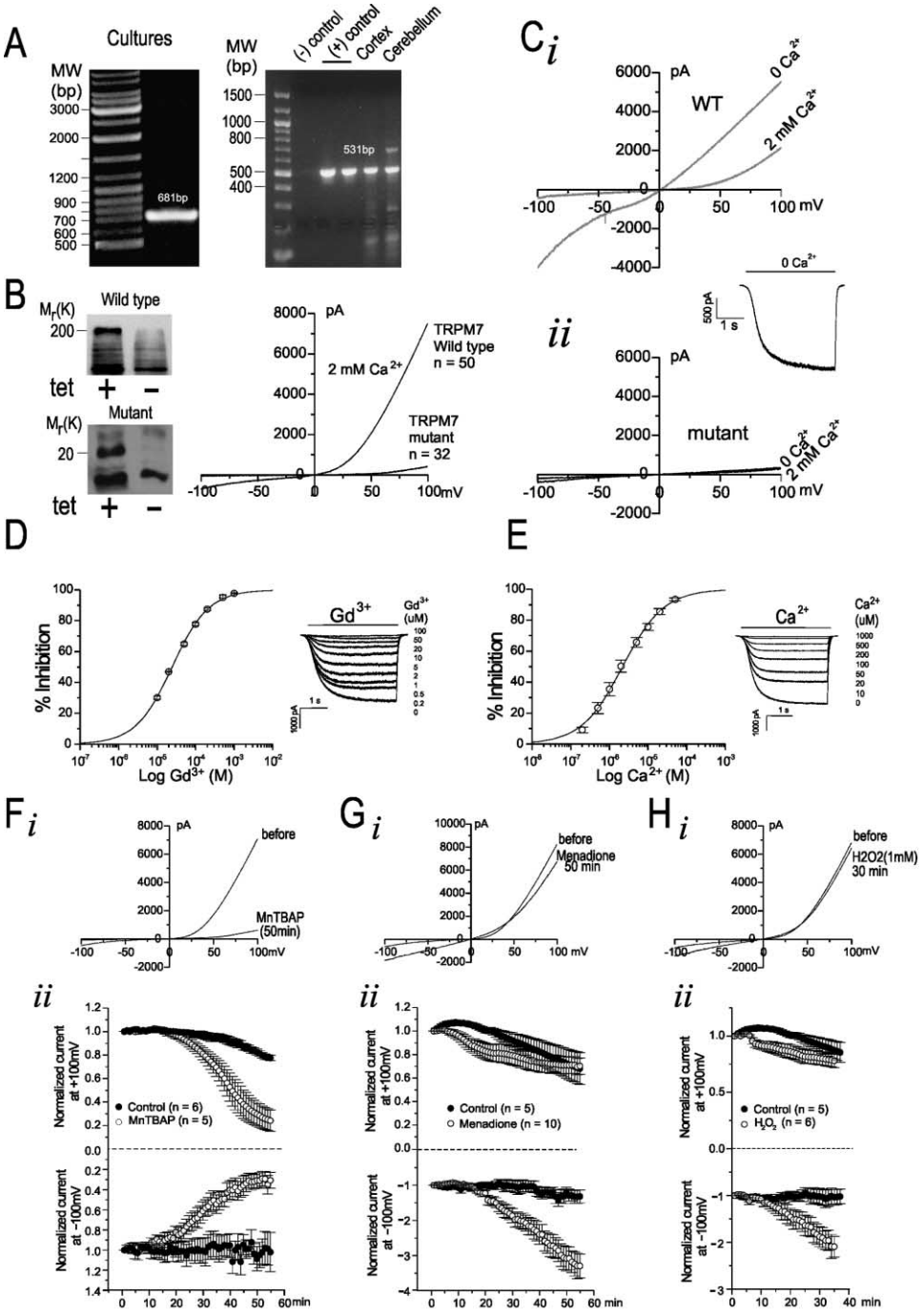

Figure 6. Expression and Characterization of TRPM7

Recordings (B–H) were made 18–24 hr after tetracycline induction of Flag-tagged murine TRPM7/pCDNA4/TO in stably transfected HEK-293 cells.

(A) RT-PCR of TRPM7 in cultured cortical neurons (left), and embryonic mouse cortex (18–19 day gestation) and 12 days postnatal mouse cerebellum (right), each gel representative of 3 experiments.

(B) Left: immunoblots of 2 HEK-293 cell lines expressing a tetracycline-controlled Flag-TRPM7 construct (wild-type, predicted size M_r 220 K) and a truncated N-terminal Flag-TRPM7 construct (mutant, Flag + aa: 0–177 of TRPM7, predicted size M_r 20 K). Right: averaged I-V curves of currents carried by HEK 293 cells after induction of wild-type and mutant TRPM7.

(C) Response to high (2 mM) and low (0 mM) extracellular Ca^{2+} of mutant (C_{ii}; n = 50) and wild-type (C_i; WT, n = 32) TRPM7. Inset: representative inward current at −60 mV, 0 $[Ca^{2+}]_e$.

(D) Inhibition of wild-type TRPM7 current by Ca^{2+} (n = 10 cells, IC_{50} for Ca^{2+} = 27.0 ± 1.53 μM). Inset: representative currents at at the indicated $[Ca^{2+}]_e$.

(E) Inhibition of wild-type TRPM7 current by Gd^{3+} (n = 9 cells, IC_{50} = 2.4 ± 0.45 μM). Inset: representative currents at the indicated $[Gd^{3+}]_e$. Inward currents in (D) and (E) were induced by reducing $[Ca^{2+}]_e$ from 2 to 0 mM at a holding potential of −60 mV.

(F) Inhibition of inward and outward currents by MnTBAP (0.2 mM in 2 mM $[Ca^{2+}]_e$).

(G) Enhancement of inward and inhibition of outward currents by menadione (0.2 mM in 2 mM $[Ca^{2+}]_e$).

(H) Enhancement of inward and inhibition of outward currents by H_2O_2 (1.0 mM in 2 mM $[Ca^{2+}]_e$). For (F–H): (*i*) representative I-V curves; (*ii*) normalized currents at +100 mV and −100 mV. Symbols are equal to mean ± SEM.

is lethal to HEK-293 cells (Nadler et al., 2001; Monteilh-Zoller et al., 2003) but can be prevented simply by elevating extracellular Mg^{2+} to restore Mg^{2+} homeostasis (Schmitz et al., 2003).

To test whether I_{OGD} corresponds to TRPM7, we first performed RT-PCR analyses on the cultured cortical neurons (Figure 6A, left), and on mouse cortex and cerebellum (Figure 6A, right). These indicated that native TRPM7 is expressed in mouse brain and was maintained in the cultures in which I_{OGD} was observed. Next we generated HEK-293 cell lines with a tetracycline-controlled expression of a Flag-tagged TRPM7 construct (Nadler et al., 2001; Monteilh-Zoller et al., 2003). As a control, we produced a Flag-tagged truncated TRPM7 construct anticipated to be devoid of channel activity (Experimental Procedures). Tetracycline induction of the transfected cells induced Flag-reactive bands with a relative molecular mass of 220,000 and 20,000 for the wild-type and mutant constructs, respectively (Figure 6B, left). As described (Nadler et al., 2001), HEK-293 cells induced to express the wild-type channel swelled, detached, and died by 72 hr. Cells induced with the mutant TRPM7 survived (data not shown). Therefore, we performed all recordings 18–48 hr after induction.

HEK-293 cells expressing wild-type TRPM7 exhibited large currents and a characteristic outwardly rectifying I-V curve, whereas those expressing mutant TRPM7 exhibited smaller currents, and a more linear I-V curve (Figure 6B). Currents in cells expressing only mutant channels were unaffected by changes in $[Ca^{2+}]_e$ (Figure $6C_{ii}$), whereas they were dramatically enhanced and lost rectification by reducing $[Ca^{2+}]_e$ in cells expressing wild-type channels (Figure $6C_i$). At -60 mV, the current was substantially inhibited by raising $[Ca^{2+}]_e$, with an IC_{50} of 27.0 ± 1.53 μM (Figure 6D). Moreover, the TRPM7 current in the absence of divalent cations could be blocked by Gd^{3+} with an IC_{50} of 2.4 ± 0.45 μM (Figure 6E). These properties are consistent with a functional expression of TRPM7 in HEK-293 cells (Nadler et al., 2001; Monteilh-Zoller et al., 2003) and with our previous observations of I_{OGD} currents in mouse neurons.

Modulation of TRPM7 Activity by ROS

I_{OGD} was activated by ROS and suppressed by ROS inhibitors (Figure 4). To test the effects of ROS on TRPM7 currents, recordings were performed in HEK-293 cells expressing wild-type TRPM7 during treatment with the SOD mimic MnTBAP, the O_2^- generator menadione, or with H_2O_2. The physiological solution contained 2 mM $[Ca^{2+}]_e$ to simulate conditions in which I_{OGD} was activated in neurons. Consistent with its effects on I_{OGD} currents and $^{45}Ca^{2+}$ uptake (Figures 4A and 4C), treatment with MnTBAP (0.2 mM) potently inhibited both inward and outward currents in the HEK-293 cells, implicating O_2^- in TRPM7 activation (Figure 6F). Menadione (0.2 mM) had a small inhibitory effect on outward TRPM7 currents, but markedly enhanced inward currents in all cells examined (Figure 6G). Similarly, H_2O_2 (1 mM) had minimal effects on outward, but markedly enhanced inward TRPM7 currents (Figure 6H). These results are consistent with effects of these ROS modulators on I_{OGD} and $^{45}Ca^{2+}$ uptake in neurons (Figure 4E), suggesting that TRPM7 is a suitable candidate for, or as a participant in, I_{OGD}.

siRNA Inhibition of TRPM7 Expression in Primary Cultured Neurons

If TRPM7 is I_{OGD} or an essential subunit of I_{OGD} in primary neurons, then suppressing TRPM7 expression should have similar consequences to blocking I_{OGD}. To suppress TRPM7 we used RNA interference (RNAi), a process of posttranscriptional gene silencing that inhibits, with high specificity, the expression of native genes in mammalian cells (Elbashir et al., 2001; Cullen, 2002). The transfection of small interfering RNA duplexes (siRNA) into primary neurons was optimized using a nonsilencing FITC-siRNA (60 pmol; Experimental Procedures). Counts indicated that 91.7% $\pm$ 1.3% of the cells (identified by Hoechst staining) were transfected ($n = 6$ experiments, mean $\pm$ SE; Figure 7A). No transfection was observed in the absence of transfection reagent. Transfected cells exhibited normal morphology and did not stain with PI, indicating good viability.

We next transfected the cultures with a 21 nucleotide siRNA duplex targeting TRPM7 ($siRNA_{TRPM7\text{-}1}$). No other known genes, including other TRP channels, exhibit sequence homology to this target sequence (GenBank search). $siRNA_{TRPM7\text{-}1}$ at 40 and 60 nM achieved complete suppression of TRPM7 mRNA 6–8 days after transfection, whereas siRNA control had no effect (Figure 7B). In previous studies, a targeted deletion of TRPM7 in a DT-40 B-cell system induced cell death within 48–72 hr (Nadler et al., 2001), suggesting a role for TRPM7 in the function of these cells. However, we did not observe adverse effects of suppressing TRPM7 in the cultured neurons by RNAi. This may be explained by Schmitz et al. (2003) who attributed the reduced viability of TRPM7-deficient HEK cells to a loss of Mg^{2+} homeostasis and who readily restored viability by supplementing extracellular Mg^{2+}. Either there was sufficient extracellular Mg^{2+} in our media and sera to maintain Mg^{2+} homeostasis in cultured neurons or there are other mechanisms in primary neurons that are capable of maintaining Mg^{2+} homeostasis in the absence of TRPM7.

To examine the specificity of the RNAi approach, we examined the effect of transfecting $siRNA_{TRPM7\text{-}1}$ on other TRPM subunits. Surprisingly, though no effects were seen on mRNA levels of TRPM6 and TRPM3, this siRNA, uniquely targeted against TRPM7, also reduced TRPM2 levels (Figure $7C_i$). To determine whether this was a nonspecific consequence of the siRNA sequence used, we generated two additional siRNAs targeting TRPM7, and exhibiting no sequence homology to any other genes (hereafter called $siRNA_{TRPM7\text{-}2}$ and $siRNA_{TRPM7\text{-}3}$; Experimental Procedures). Transfecting primary cortical neurons with each of these had the identical effect to $siRNA_{TRPM7\text{-}1}$ of also suppressing TRPM2 mRNA, without effects on TRPM3 and TRPM6. This argues against nonspecific effects of RNAi and raises the possibility that TRPM7 and TRPM2 expression are interdependent. This might be explained if native channels containing TRPM7 formed heteromers that also include TRPM2, a possibility recently supported by analogous findings for native TRPC channels (Strubing et al., 2003).

RNAi Inhibits TRPM7-Mediated Currents in Primary Cultured Neurons

If neuronal I_{OGD} requires TRPM7 then suppressing TRPM7 should specifically inhibit I_{OGD}-like currents. We

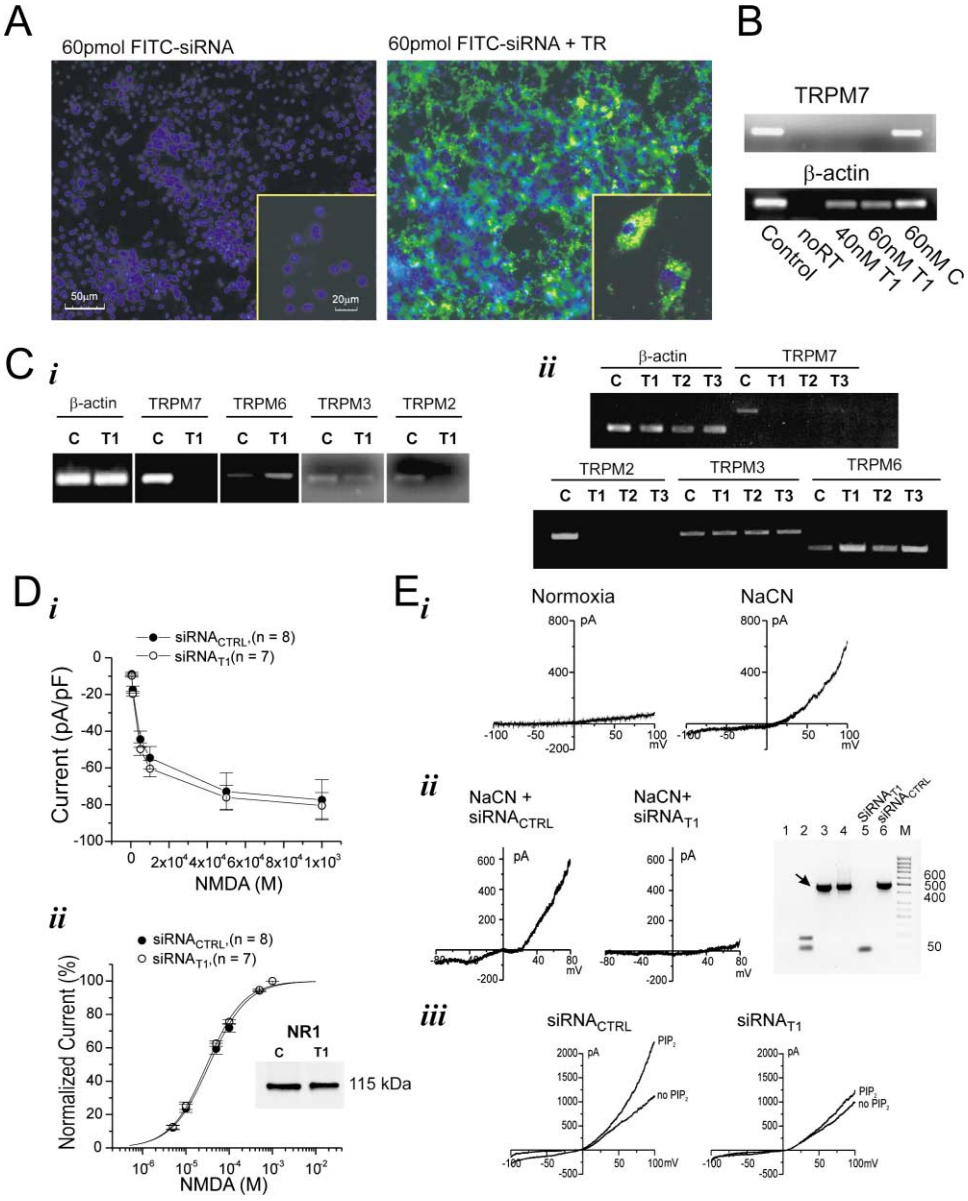

Figure 7. siRNA Inhibition of TRPM7 in Primary Cultured Neurons

(A) High-efficiency transfection of FITC-labeled siRNA (green) in cultured cortical neurons at 12 days. Cell nuclei were counterstained with Hoechst 33352 (blue). Scale bar is equal to 50 μm. Insets: higher power view illustrating intracellular localization of transfected siRNA. Scale bar is equal to 20 μm.

(B) TRPM7 expression in primary cortical cultures 6 days after transfection with siRNA$_{TRPM7\text{-}1}$ (T1). TRPM7 expression was determined by RT-PCR. C: control siRNA. TRPM7 expression for each sample was compared against β-actin (C). Effect of siRNA$_{TRPM7\text{-}1}$ (C$_i$) and of siRNA$_{TRPM7\text{-}1to3}$ (T1-T3; C$_{ii}$) on the expression of the indicated TRPM proteins. C: control siRNA.

(D) Effect of control siRNA and siRNA$_{TRPM7\text{-}1}$ on peak (D$_i$) and normalized (D$_{ii}$) NMDA currents, and on NR1 NMDAR subunit expression by immunoblotting (D$_{ii}$, inset; representative of three experiments).

(E) Suppression of I_{OGD} and TRPM-like currents in cultured neurons by RNAi. Mg^{2+} was omitted from the patch pipette to enhance TRPM7 currents (0 Mg^{2+}, 5 mM ATP). (E$_i$) recordings of enhanced I_{OGD} (Gd^{3+}-sensitive) currents by Mg^{2+}-free pipette solutions in controls and chemically anoxic neurons (Representative of nine neurons/condition, compare with Figure 3B). (E$_{ii}$) I_{OGD} currents and single-cell PCR from chemically anoxic cultured neurons treated with control siRNA or siRNA$_{TTRPM7\text{-}1}$. Gel: single-cell RT-PCR for TRPM7 message (arrow). Lanes are 1, negative control; 2, control using all reagents but no cell contents; 3 and 4, message from single CA1 pyramidal neurons dissociated from adult rat hippocampus; 5 and 6, message from the siRNA$_{T1}$ and control neurons shown in the middle and left images, respectively (representative of eight experiments). (E$_{iii}$) effect of inhibiting TRPM7 by RNAi on the enhancement PIP_2-induced currents (representative of n = 11 control and 22 siRNA$_{T1}$-treated cells).

first examined the effect of inhibiting TRPM7 on NMDAR currents and NR1 subunit expression (Figure 7D$_{i,ii}$). Neither was affected by the siRNA$_{TRPM7\text{-}1}$ treatment, suggesting no interference with NMDARs. Next, we determined whether TRPM7-dependent channels mediate I_{OGD} in cultured neurons. In cell lines, TRPM7 currents

are subject to a slowly developing disinhibition ("runup") by low intracellular Mg^{2+} concentration, or inhibition ("rundown") by high intracellular Mg^{2+} (Kozak and Cahalan, 2003). Thus, we recorded I_{OGD} in neurons exposed to chemical anoxia using patch pipettes containing a Mg^{2+} free solution to minimize the intracellular inhibition of endogenous TRPM7-dependent currents. Following patch breakthrough, I_{OGD} consistently increased in amplitude ($n = 9$, data not shown) over 5 to 15 min. In contrast, a high Mg^{2+} patch pipette solution (6 mM Mg^{2+}, 0 ATP) resulted in rundown of this current ($n = 9$, data not shown) consistent with the inhibition of TRPM7 by intracellular Mg^{2+}. The use of a Mg^{2+}-free pipette solution substantially enhanced I_{OGD} (Figure 7E$_i$, compare with Figure 3B) and was therefore used to examine the effect of RNAi silencing of TRPM7 on I_{OGD}.

SiRNA-transfected neurons were exposed to chemical anoxia, patch recordings were made, and TRPM7 message was subsequently examined in the same cells by single cell RT-PCR (Experimental Procedures). Neurons treated with control siRNA exhibited robust I_{OGD} currents in response to NaCN whereas those treated with $siRNA_{TRPM7\text{-}1}$ showed no I_{OGD}. Moreover, neurons exhibiting I_{OGD} were positive for TRPM7 message, whereas it was lacking in neurons not exhibiting I_{OGD} (Figure 7E$_{ii}$). This confirms the dependence of I_{OGD} on TRPM7.

Next, we exploited the potential activation of endogenous TRPM7 channels by including phosphatidyliositol-4,5-bisphosphate (PIP_2) in patch pipettes (Runnels et al., 2002). With PIP_2 in cultured neurons we observed a runup of the PIP_2-induced currents when Mg^{2+} was excluded from the patch pipette and a rundown when a high concentration (6 mM) was included in the pipette (data not shown). The intracellular PIP_2 substantially enhanced voltage-ramp currents while treatment of the cells with siRNA for TRPM7 strongly depressed this current (Figure 7E$_{iii}$). In control cells, the inward and outward currents measured at -90 and $+90$ mV, respectively, were -55 ± -14 pA (mean, S.E.M.) and 1095 ± -150 pA ($n = 11$). With PIP_2 in the pipette the comparable values were -153 ± 31 and 1640 ± 101 pA ($n = 11$). siRNA suppression of TRPM7 in cortical cultures suppressed the PIP_2-induced currents in a majority of neurons tested. The mean difference in inward current was -98 pA ($n = 11$) for control siRNA and -12 pA ($n = 22$) for $siRNA_{T1}$ at -90 mV; and, at $+90$ mV they were 545 pA and 56 pA, respectively ($p < 0.01$; ANOVA).

TRPM7 and TRPM2 channels share the property of modulation by ROS (Hara et al., 2002; Wehage et al., 2002), and we have shown that siRNA targeted against TRPM7 may also inhibit TRPM2 mRNA (Figure 7C). However, I_{OGD} currents in neurons exhibit outwardly rectifying I-V curves, are enhanced by low Ca^{2+}, low Mg^{2+} and PIP_2, and are inhibited by high Mg^{2+}; all properties that are not shared by TRPM2 channels (reviewed in Perraud et al., 2003). Thus, though it is possible that I_{OGD} channels are heteromers that also include other TRPM subunits, our data suggest that TRPM7 is a major component of I_{OGD}.

siRNA against TRPM7 Protects Anoxic Neurons by Inhibiting ROS Production and Ca^{2+} Uptake

Our data thus far suggest that the mechanism of anoxic Ca^{2+} uptake involves a positive feedback loop whereby Ca^{2+} entry through I_{OGD} stimulates ROS (NO and O_2^-) that further activate I_{OGD}, and that TRPM7 is a key component of I_{OGD} (Figure 8D). Elevating $[Ca^{2+}]_i$ or ROS independently of I_{OGD} also fed into and accelerated this loop, as evidenced by the rapidity of Ca^{2+} uptake when NMDAR activity was permitted during OGD (Figures 1B and 1C), when ROS donors were used (Figure 4G), or when endogenous ROS production was incited even in the absence of anoxia (Figure 4E) . Thus, if TRPM7 is a key component of this loop, then suppressing TRPM7 should inhibit ROS production independently of anoxia. To test this, we examined the impact of suppressing TRPM7 on ROS production initiated by an NO donor. Cortical neuronal cultures were transfected with $siRNA_{TRPM7\text{-}1}$ or with the nonsilencing control siRNA ($siRNA_{CTRL}$). They were treated under normoxic conditions with the NO donor sodium nitroprosside (SNP; 300 μM; Sattler et al., 1999). ROS production was measured by monitoring the oxidation of nonfluorescent dihydrorhodamine 123 to fluorescent rhodamine 123 (Dugan et al., 1995). Fluorescence measurements over a 2 hr SNP exposure revealed that suppressing TRPM7 expression attenuated overall ROS production in the neurons (Figure 8A), supporting a role for TRPM7 in this process.

Next, we examined the effect of TRPM7 inhibition on $^{45}Ca^{2+}$ uptake in cortical neurons during OGD (0–3 hr). All procedures were performed as in prior experiments (Figure 1B) except that the cultures were transfected with siRNAs. OGD without MCN evoked substantial $^{45}Ca^{2+}$ uptake in neurons transfected with the $siRNA_{CTRL}$ as it did previously in untransfected cells (compare with OGD without MCN in Figure 1B). However, suppressing TRPM7 significantly inhibited $^{45}Ca^{2+}$ accumulation evoked by all OGD durations (Figure 8B). Importantly, the inhibition of $^{45}Ca^{2+}$ uptake was observed in $siRNA_{TRPM7\text{-}1}$-treated neurons even in the absence of AET (MCN), and this was evident even in the first hour of anoxia. As suppressing TRPM7 did not affect NMDA currents in these cells (Figure 7D), the reduced Ca^{2+} accumulation in the absence of NMDA blockers suggests that much of the total Ca^{2+} uptake was mediated by TRPM7-dependent channels and not by NMDARs.

Lastly, we examined the effect of TRPM7 inhibition on the survival of cortical neurons in anoxia. Cultures transfected with siRNAs were exposed to OGD (0–3 hr), and cell death was gauged at 24 hr as in prior experiments (Figure 1A). As previously observed, neurons exposed to 1 hr OGD in the absence of MCN succumbed by 24 hr, whereas those treated with MCN survived (Figure 8C, compare with Figure 1A). However, neurons lacking TRPM7 were resilient to OGD even in the absence of AET, and this was already evident in the first hour of OGD. This was consistent with the effect of TRPM7 suppression on $^{45}Ca^{2+}$ uptake during 1–3 hr OGD with or without MCN (Figure 8B), but contrasts with the usual lethal effect of OGD on cortical neurons (Figure 1A and Goldberg and Choi, 1993). Moreover, a significant proportion of neurons lacking TRPM7 survived OGD exposures of up to 3 hr, regardless of whether they had also been treated with antiexcitotoxic agents (Figure 8C). Thus, TRPM7 is important to toxicity in all OGD durations, and suppressing TRPM7 permits the extended survival of anoxic neurons that were otherwise

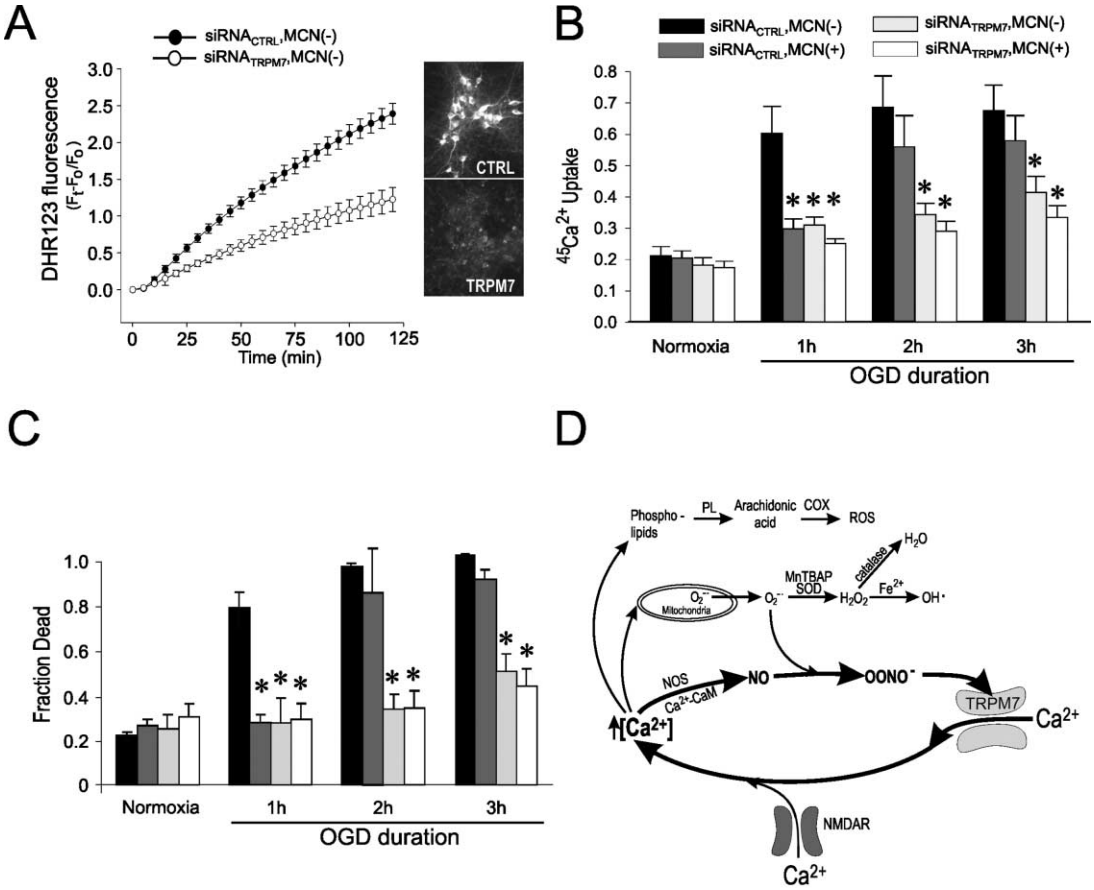

Figure 8. siRNA Inhibition of TRPM7 Permits Survival of Neurons Otherwise Destined to Die from OGD

(A) TRPM7 suppression reduces ROS production in neurons exposed to SNP (300μM). Symbols are equal to mean ± SE of 14 cultures/group in two experiments. Inset: DHR fluorescence in neurons from each group at 30 min.

(B and C) Effect of inhibiting TRPM7 on neuronal $^{45}Ca^{2+}$ uptake (B) and survival (C) in OGD. Cell death was gauged at 24 hr, $^{45}Ca^{2+}$ accumulation was measured when the exposure was terminated. Experiments were performed in the presence [MCN(+)] or absence [MCN(−)] of antagonists. Scale bars are equal to mean ± SEM of four experiments. Asterisk: different from siRNA$_{CTRL}$, MCN(−), (Bonferroni t test, $p < 0.001$).

(D) Schematic of the mechanism of anoxic neuronal death. PL, phospholipase; COX, cyclooxygenase.

destined to die. Taken together, our data show that TRPM7-containing channels, not excitotoxicity, are rate limiting in anoxic neuronal death.

Discussion

The data suggest that excitotoxicity is a subset of a larger neurotoxic mechanism that involves a regenerative Ca^{2+}-dependent cellular ROS production maintained by I_{OGD}/TRPM7 activity (Figure 8D). In support of this is that suppressing TRPM7, NO, and O_2^- resulted in reduced $^{45}Ca^{2+}$ uptake and cell death following anoxia (Figures 4, 5, and 8B), whereas increasing NO or O_2^- production with NO donors or mitochondrial O_2^- generators, respectively, enhanced $^{45}Ca^{2+}$ uptake and I_{OGD}/TRPM7 activity (Figures 4E, 4G, and 6G). Also neuronal ROS production was inhibited when TRPM7 expression was suppressed (Figure 8A), indicating an interdependence between ROS production and TRPM7 that is explained by a positive feedback loop in which ROS production is reinforced by Ca^{2+} entry through I_{OGD} (Figure 8D). It is still unknown whether a given ROS species is more effective than others in activating I_{OGD}. However, the NO pathway is predominantly responsible for generating these ROS because inhibitors and activators of alternative pathways did not affect I_{OGD} currents, $^{45}Ca^{2+}$ uptake, or cell death.

We propose that anoxia triggers both excitotoxicity and I_{OGD}. However, anoxia suppresses synaptic activity (Figures 2A–2C), consistent with observations that in cerebral ischemia, spontaneous neuronal activity, and excitability are suppressed, and no hyperactivity is observed even after reperfusion (Gao et al., 1998). In addition, glutamate receptors will desensitize (Figure 2D) and reduce the impact of anoxic glutamate release by synaptic and nonsynaptic mechanisms. Excitotoxicity may thus become less important with increasing durations of anoxia. As NMDARs exhibit significant Ca^{2+} permeability, it is likely that their early activation in anoxia accelerates the feedback loop involving Ca^{2+} excess and NO-mediated ROS production, as suggested by a more rapid rise in $[Ca^{2+}]_i$ in anoxic neurons in the absence of MCN (Figure 1C). However, the effectiveness of TRPM7 suppression in blocking $^{45}Ca^{2+}$ uptake and

anoxic death in the absence of MCN (Figures 8B and 8C) also suggests that I_{OGD} channels, not NMDARs, are the dominant pathways of neurotoxic Ca^{2+} influx in anoxia. This may explain why AET averts neuronal death after brief anoxic insults but fails when anoxia is prolonged.

Unique among ion channels, TRPM7 has a functional C-terminal kinase, though the role of this is unclear (Runnels et al., 2001; Nadler et al., 2001; Kozak and Cahalan, 2003). The I/V characteristics, block by polyvalent cations, enhancement by low Ca^{2+} and PIP_2, and modulation by ROS make TRPM7 the likeliest candidate for I_{OGD}. However, other ion channels, especially TRPM2, could produce anoxic neuronal damage. TRPM2 shares amino acid homology with TRPM7, is also widely expressed in brain and other organs, and is activated by H_2O_2 and reactive nitrogen species (Hara et al., 2002; Wehage et al., 2002). Our data (Figure 7C) raise the possibility I_{OGD} is a heteromeric cation conductance containing TRPM7, but also other TRP channel subunits such as TRPM2. Addressing other TRP channels in the future may clarify their role in anoxic injury and possibly permit a further increase in the anoxic tolerance of neurons.

Our data also do not exclude a neurotoxic role for ions other than Ca^{2+} in I_{OGD} neurotoxicity. Indeed, heterologously overexpressed TRPM7 channels in HEK-293 cells conduct a range of divalent cations with a strong preference for Zn^{2+} and Ni^{2+}, which permeate the channel even better than Ca^{2+} (Monteilh-Zoller et al., 2003). Some of the ions that permeate through TRPM7, especially Zn^{2+}, have been previously implicated in ischemic brain damage (reviewed in Choi and Koh, 1998). However, past studies have focused on glutamate receptors as the suggested route of cellular Zn^{2+} entry (Weiss et al., 1993; Sensi et al., 1999), though some have hinted at other, less characterized pathways (Sheline et al., 2002). Our findings implicate TRPM7 as the key route for cellular entry of toxic cations.

Our report provides a paradigm for understanding anoxic neuronal damage, which is consistent with all previous basic and clinical research on anoxic mechanisms. The data may explain the dichotomy between the success of AET in laboratory models of neurological disease, and its failure in human clinical trials. The mechanisms described here strongly suggest that AET treats only a subset of a larger process in which I_{OGD}/TRPM7 activity is ultimately neurotoxic. Under this hypothesis, treating excitotoxicity would slow anoxic neuronal damage, but would not prevent it when the anoxia is severe. It is possible that patients enrolled in failed trials of AET for stroke or traumatic brain injury were selected to have severe injuries (Morris et al., 1999), or that these disorders in humans, by their nature, induce severe ischemia. Thus, future treatment of such disorders may also need to inhibit I_{OGD}/TRPM7. This will address both the excitotoxic trigger, and the predominant mechanism that perpetuates the damage.

Experimental Procedures

Tissue Culture

Mixed cortical cell cultures enriched with neurons (>85%) were prepared as previously described (Sattler et al., 1997, 1998) and used for experiments after 12–14 days in vitro.

Drugs and Solutions

The control solution contained (in mM): 121 NaCl, 5 KCl, 20 D-glucose, 10 HEPES acid, 7 HEPES-Na salt, 3 $NaHCO_3$, 1 Na-pyruvate, 1.8 $CaCl_2$, and 0.01 glycine, adjusted to pH 7.4 with NaOH. OGD was performed in a glucose-free bicarbonate-buffered solution containing (in mM): 121 NaCl, 5 KCl, 1 Na-pyruvate, 1.8 $CaCl_2$, 25 $NaHCO_3$, 0.01 glycine, adjusted to pH 7.4 with HCl. Stocks of nimodipine (Miles Pharmaceuticals), 6-cyano-7-nitroquinoxaline (CNQX; Research Biochemicals) and dihydrorhodamine (DHR; Molecular Probes) were prepared in DMSO. Ketamine, APV, MK-801, and propidium iodide (PI) stocks were prepared in distilled water. All were stored at −20°C until used. All other compounds were diluted to their final concentrations directly in the experimental solution.

Determination of Cell Death and ROS Production

Cell death and ROS were determined by fluorescence measurements of PI (50 μg/ml) and DHR (10 μM), respectively, using a multiwell plate fluorescence scanner (CytoFluor II, PerSeptive Biosytems; Sattler et al., 1997). The fraction of dead cells in each culture was calculated as: fraction dead = $(F_t - F_o)/F_{NMDA}$ Where F_t = PI fluorescence at time t, F_o = initial PI fluorescence and F_{NMDA} = background subtracted PI fluorescence of sister cultures 24 hr after a 60 min exposure to 1 mM NMDA at 37°C.

Oxygen-Glucose Deprivation (OGD)

The cultures were transferred to an anaerobic chamber containing a 5% CO_2, 10% H_2, and 85% N_2 (<0.2%O_2) atmosphere (Goldberg and Choi, 1993). They were washed 3× with 500 μl of deoxygenated glucose-free bicarbonate solution and maintained anoxic for the appropriate duration at 37°C. OGD was terminated by washing the cultures with oxygenated glucose-containing (20 mM) bicarbonate solution. The cultures were maintained for a further 21–23 hr at 37°C in a humidified 5% CO_2 atmosphere.

Measurements of Ca^{2+} Loading

$^{45}Ca^{2+}$ uptake was measured as described (Sattler et al., 1998). In brief, $^{45}CaCl_2$ (0.85 μCi/well, 0.5–0.6 mM) was added to the anoxic solution used during OGD. After the insult, the cells were rinsed 4× in cold control solution, lysed with 0.2% sodium dodecyl sulfate, and counted in a scintillation counter. $^{45}Ca^{2+}$ counts were normalized to those obtained from sister cultures exposed to 1 mM NMDA for 1 hr. $[Ca^{2+}]_i$ during OGD was determined as previously described (Tymianski et al., 1993; Sattler et al., 1998) by imaging neurons loaded with the low Ca^{2+}-affinity indicator fura-2/FF (Golovina and Blaustein, 1997) . The neurons were mounted in a sealed chamber of a microscope stage incubator at 37°C that permitted exchanges of anoxic and oxygenated solutions and gases.

TRPM7 Mutant Construct

The Flag–murineTRPM7/pCDNA4-TO cDNA (kind gift of A. Scharenberg, Seattle WA) was digested by PstI/XbaI, blunted and self-ligated, leaving in the construct only 570 bp of the TRPM7 sequence expressing 190 aa of Flag + N terminus TRPM7.

Electrophysiology

Recordings in Neurons

Whole-cell patch-clamp recordings were performed and analyzed previously described (Xiong et al., 1997). Following whole-cell formation, the I-V relationship was obtained with a 2.5 s voltage ramp pulse applied from −100 mV to +80 mV. During each experiment a voltage step of −10 mV was applied from holding potential (−60 mV) and the cell capacitance was calculated by integrating the capacitative transient. Only recordings with a pipette-membrane seal > 2 GΩ were included. The extracellular solution (ECF) contained (in mM): 140 NaCl, 5.4 KCl, 1.3 $CaCl_2$, 25 HEPES, 0.001 tetrodotoxin, 20 μM MK801, 40 μM CNQX, and 5 μM nimodipine (pH 7.4, 320–335 mOsm adjusted with sucrose). The pipette solution contained (in mM): 140 CsF (or CsCl), 35 CsOH, 10 HEPES, 2 tetraethylammonium chloride (TEA), 5 EGTA, 1 $CaCl_2$, pH 7.3 at 300 mOsm. To evoke I_{OGD} currents, cells were incubated for 2 hr with glucose-free ECF containing 3 mM NaCN. NaCN was then washed away and the recordings performed within 1 hr. No obvious recovery of the NaCN effect was observed within this period.

Recordings in HEK-293 Cells

HEK-293 cells transfected with the Flag-murine TRPM7/pCDNA4-TO or the mutant Flag-murine TRPM7 construct were grown on glass coverslips with DMEM supplemented with 10% fetal bovine serum, blasticidin (5 μg/ml), and zeocin (0.4 mg/ml). TRPM7 expression was induced by adding 1 μg/ml tetracycline to the culture medium (Nadler et al., 2001). Whole-cell patch-clamp experiments were performed 18–48 hr after induction. Following whole-cell formation, the I-V relationship was obtained with a 500 ms voltage ramp pulse applied from −100 mV to +100 mV. The holding potential was 0 mV. The extracellular solution (ECF) contained (in mM): 140 NaCl, 5.4 KCl, 2 $CaCl_2$, 25 HEPES, and 33 glucose. The pH was adjusted to 7.4 with NaOH. The pipette solution contained (in mM): 145 Cs-methanesulphonate, 8 NaCl, 5 ATP, 1 $MgCl_2$, EGTA 10, 4.1 $CaCl_2$, and 10 HEPES. The pH was adjusted to 7.3 with CsOH.

siRNA Reagents

To determine transfection efficacy, we used a nonsilencing FITC-conjugated siRNA control, sequence AAT TCT CCG AAC GTG TCA CGT, with a 5′ fluorescein tag on the sense strand (Xeragon). The siRNAs against TRPM7 corresponded to coding regions 5152–5172, 5023–5043, and 1318–1338 ($siRNA_{TRPM7\text{-}1}$ to $siRAN_{TRPM7\text{-}3}$, respectively) relative to the first nucleotide of the start codon of murine TRPM7 (GenBank accession number AY032951). The $siRNA_{CTRL}$ was a commercially available nonsilencing sequence (siRNA Negative Control #1, cat# 4610 Ambion Inc.).

siRNA Transfection

On day six in culture, the cortical neurons were transfected with 60 pmol siRNA (control or TRPM7) using the GeneSilencer siRNA Transfection Reagent (Gene Therapy Systems) and following the manufacturer's suggestions. In brief, siRNA and GeneSilencer were each diluted to 100 μL with OptiMEM (Invitrogen Life Technologies) and then mixed together for 10 min. Cells were fed 1 mL fresh culture medium and overlaid with the transfection mix. After 24 hr, the cells were fed with 2 mL culture medium. Transfected cells were used for experiments or harvested for RNA 12–14 days after plating.

Single-Cell PCR

At the end of a patch recording, the cell contents were aspirated into the pipette and expelled into an Eppendorf tube containing 1 U of RNase inhibitor. cDNA was reverse transcribed using Superscript II RT (Invitrogen Life Technologies) with oligo(dT). TRPm7 expression was determined using the following oligonucleotide primers: forward (5′-aggagaatgtcccagaaatcc) reverse: (5′-tcctccag ttaaaatccaagc) to yield a 531 estimated fragment size. 5 μl of the first round of PCR was used for a second round with 30 cycles of amplification. The amplified product was purified and automatically sequenced (Beckman CEQ 2000) using the same primers. The PCR product sequence was checked against the TRPm7 cDNA (sequence AY032951) and found to produce full alignment within 495 bp in the forward and reverse strands.

Acknowledgments

Supported by NIH Grant NS 39060 (M.T.), the Ontario Heart and Stroke Foundation, Canadian Institutes of Health Research (CIHR), and the Canadian Stroke Networks (M.T., J.F.M.). M.A. is a fellow of the Ontario Heart and Stroke Foundation. M.A. is a student and M.T. a Clinician-Scientist of the CIHR. We thank Drs. M.P. Goldberg, M.W. Salter, Y.T. Wang and L. Schlichter for a critical review of the manuscript; Dr. David Nicholls for useful discussions about chemical anoxia; Chang Bai Liu and E. Czerwinska for technical assistance; and Dr. A. Scharenberg for the Flag–murine TRPM7/pCDNA4-TO cDNA.

Received: May 15, 2003
Revised: November 14, 2003
Accepted: November 14, 2003
Published: December 24, 2003

References

Aarts, M., Liu, Y., Liu, L., Besshoh, S., Arundine, M., Gurd, J.W., Wang, Y.T., Salter, M.W., and Tymianski, M. (2002). Treatment of ischemic brain damage by perturbing NMDA receptor-PSD-95 protein interactions. Science *298*, 846–850.

Birmingham, K. (2002). Future of neuroprotective drugs in doubt. Nat. Med. *8*, 5.

Budd, S.L., and Nicholls, D.G. (1996). A reevaluation of the role of mitochondria in neuronal Ca2+ homeostasis. J. Neurochem. *66*, 403–411.

Choi, D.W., and Koh, J.Y. (1998). Zinc and brain injury. Annu. Rev. Neurosci. *21*, 347–375.

Choi, D.W., Maulucci-Gedde, M., and Kriegstein, A.R. (1987). Glutamate neurotoxicity in cortical cell culture. J. Neurosci. *7*, 357–368.

Cullen, B.R. (2002). RNA interference: antiviral defense and genetic tool. Nat. Immunol. *3*, 597–599.

Davis, S.M., Albers, G.W., Diener, H.C., Lees, K.R., and Norris, J. (1997). Termination of acute stroke studies involving selfotel treatment. ASSIST Steering Committed. Lancet *349*, 32.

Dugan, L.L., Sensi, S.L., Canzoniero, L.M.T., Handran, S.D., Rothman, S.M., Lin, T.S., Goldberg, M.P., and Choi, D.W. (1995). Mitochondrial production of reactive oxygen species in cortical neurons following exposure to N-methyl-D-aspartate. J. Neurosci. *15*, 6377–6388.

Elbashir, S.M., Harborth, J., Lendeckel, W., Yalcin, A., Weber, K., and Tuschl, T. (2001). Duplexes of 21-nucleotide RNAs mediate RNA interference in cultured mammalian cells. Nature *411*, 494–498.

Gao, T.M., Pulsinelli, W.A., and Xu, Z.C. (1998). Prolonged enhancement and depression of synaptic transmission in CA1 pyramidal neurons induced by transient forebrain ischemia in vivo. Neuroscience *87*, 371–383.

Goldberg, M.P., and Choi, D.W. (1993). Combined oxygen and glucose deprivation in cortical cell culture: calcium-dependent and calcium-independent mechanisms of neuronal injury. J. Neurosci. *13*, 3510–3524.

Goldberg, M.P., Weiss, J.H., Pham, P.C., and Choi, D.W. (1987). N-methyl-D-aspartate receptors mediate hypoxic neuronal injury in cortical culture. J. Pharmacol. Exp. Ther. *243*, 784–791.

Golovina, V.A., and Blaustein, M.P. (1997). Spatially and functionally distinct Ca2+ stores in sarcoplasmic and endoplasmic reticulum. Science *275*, 1643–1648.

Hara, Y., Wakamori, M., Ishii, M., Maeno, E., Nishida, M., Yoshida, T., Yamada, H., Shimizu, S., Mori, E., Kudoh, J., et al. (2002). LTRPC2 Ca2+-permeable channel activated by changes in redox status confers susceptibility to cell death. Mol. Cell *9*, 163–173.

Ikonomidou, C., and Turski, L. (2002). Why did NMDA receptor antagonists fail clinical trials for stroke and traumatic brain injury? Lancet Neurol. *1*, 383–386.

Kerschbaum, H.H., Kozak, J.A., and Cahalan, M.D. (2003). Polyvalent cations as permeant probes of MIC and TRPM7 pores. Biophys. J. *84*, 2293–2305.

Kozak, J.A., and Cahalan, M.D. (2003). MIC channels are inhibited by internal divalent cations but not ATP. Biophys. J. *84*, 922–927.

Lees, K.R., Asplund, K., Carolei, A., Davis, S.M., Diener, H.C., Kaste, M., Orgogozo, J.M., and Whitehead, J. (2000). Glycine antagonist (gavestinel) in neuroprotection (GAIN International) in patients with acute stroke: a randomised controlled trial. Lancet *355*, 1949–1954.

Lipton, P. (1999). Ischemic cell death in brain neurons. Physiol. Rev. *79*, 1431–1568.

Lipton, S.A., and Rosenberg, P.A. (1994). Excitatory amino acids as a final common pathway for neurologic disorders. N. Engl. J. Med. *330*, 613–622.

Monteilh-Zoller, M.K., Hermosura, M.C., Nadler, M.J., Scharenberg, A.M., Penner, R., and Fleig, A. (2003). TRPM7 provides an ion channel mechanism for cellular entry of trace metal ions. J. Gen. Physiol. *121*, 49–60.

Montell, C., Birnbaumer, L., and Flockerzi, V. (2002). The TRP channels, a remarkably functional family. Cell *108*, 595–598.

Morris, G.F., Bullock, R., Marshall, S.B., Marmarou, A., Maas, A., and Marshall, L.F. (1999). Failure of the competitive N-methyl-D-aspartate antagonist selfotel (CGS 19755) in the treatment of se-

vere head injury: results of two phase III clinical trials. J. Neurosurg. *91*, 737–743.

Nadler, M.J., Hermosura, M.C., Inabe, K., Perraud, A.L., Zhu, Q., Stokes, A.J., Kurosaki, T., Kinet, J.P., Penner, R., Scharenberg, A.M., and Fleig, A. (2001). LTRPC7 is a Mg.ATP-regulated divalent cation channel required for cell viability. Nature *411*, 590–595.

Olney, J.W. (1969). Brain lesion, obesity and other disturbances in mice treated with monosodium glutamate. Science *164*, 719–721.

Patel, M., Day, B.J., Crapo, J.D., Fridovich, I., and McNamara, J.O. (1996). Requirement for superoxide in excitotoxic cell death. Neuron *16*, 345–355.

Perraud, A.L., Schmitz, C., and Scharenberg, A.M. (2003). TRPM2 Ca2+ permeable cation channels: from gene to biological function. Cell Calcium *33*, 519–531.

Rossi, D.J., Oshima, T., and Attwell, D. (2000). Glutamate release in severe brain ischaemia is mainly by reversed uptake. Nature *403*, 316–321.

Runnels, L.W., Yue, L., and Clapham, D.E. (2001). TRP-PLIK, a bifunctional protein with kinase and ion channel activities. Science *291*, 1043–1047.

Runnels, L.W., Yue, L., and Clapham, D.E. (2002). The TRPM7 channel is inactivated by PIP(2) hydrolysis. Nat. Cell Biol. *4*, 329–336.

Sattler, R., Charlton, M.P., Hafner, M., and Tymianski, M. (1997). Determination of the time-course and extent of neurotoxicity at defined temperatures in cultured neurons using a modified multi-well plate fluorescence scanner. J. Cereb. Blood Flow Metab. *17*, 455–463.

Sattler, R., Charlton, M.P., Hafner, M., and Tymianski, M. (1998). Distinct influx pathways, not calcium load, determine neuronal vulnerability to calcium neurotoxicity. J. Neurochem. *71*, 2349–2364.

Sattler, R., Xiong, Z., Lu, W.Y., Hafner, M., MacDonald, J.F., and Tymianski, M. (1999). Specific coupling of NMDA receptor activation to nitric oxide neurotoxicity by PSD-95 protein. Science *284*, 1845–1848.

Schmitz, C., Perraud, A.L., Johnson, C.O., Inabe, K., Smith, M.K., Penner, R., Kurosaki, T., Fleig, A., and Scharenberg, A.M. (2003). Regulation of vertebrate cellular Mg2+ homeostasis by TRPM7. Cell *114*, 191–200.

Sensi, S.L., Yin, H.Z., and Weiss, J.H. (1999). Glutamate triggers preferential Zn2+ flux through Ca2+ permeable AMPA channels and consequent ROS production. Neuroreport *10*, 1723–1727.

Sheline, C.T., Ying, H.S., Ling, C.S., Canzoniero, L.M., and Choi, D.W. (2002). Depolarization-induced 65zinc influx into cultured cortical neurons. Neurobiol. Dis. *10*, 41–53.

Simon, R.P., Swan, J.H., and Meldrum, B.S. (1984). Blockade of N-methyl-D-aspartate receptors may protect against ischemic damage in the brain. Science *226*, 850–852.

Strubing, C., Krapivinsky, G., Krapivinsky, L., and Clapham, D.E. (2003). Formation of novel TRPC channels by complex subunit interactions in embryonic brain. J. Biol. Chem. *278*, 39014–39019.

Tymianski, M., Charlton, M.P., Carlen, P.L., and Tator, C.H. (1993). Source specificity of early calcium neurotoxicity in cultured embryonic spinal neurons. J. Neurosci. *13*, 2085–2104.

Wehage, E., Eisfeld, J., Heiner, I., Jungling, E., Zitt, C., and Luckhoff, A. (2002). Activation of the cation channel long transient receptor potential channel 2 (LTRPC2) by hydrogen peroxide. A splice variant reveals a mode of activation independent of ADP-ribose. J. Biol. Chem. *277*, 23150–23156.

Weiss, J.H., Hartley, D.M., Koh, J.Y., and Choi, D.W. (1993). AMPA receptor activation potentiates zinc neurotoxicity. Neuron *10*, 43–49.

Xiong, Z., Lu, W., and MacDonald, J.F. (1997). Extracellular calcium sensed by a novel cation channel in hippocampal neurons. Proc. Natl. Acad. Sci. USA *94*, 7012–7017.

Ying, W., Anderson, C.M., Chen, Y., Stein, B.A., Fahlman, C.S., Copin, J.C., Chan, P.H., and Swanson, R.A. (2000). Differing effects of copper, zinc superoxide dismutase overexpression on neurotoxicity elicited by nitric oxide, reactive oxygen species, and excitotoxins. J. Cereb. Blood Flow Metab. *20*, 359–368.